Composite MR image reconstruction and unaliasing for general trajectories using Neural Networks

Neelam Sinha*,[1], A. G. Ramakrishnan, Manojkumar Saranathan

Department of Electrical Engineering, Indian Institute of Science, Bangalore, India-560012

Abstract

In rapid parallel MR imaging, the problem of image reconstruction is challenging. Here, a novel image reconstruction technique for data acquired along any general trajectory in neural network framework, called "Composite Reconstruction And Unaliasing using Neural Networks" (CRAUNN), is proposed. CRAUNN is based on the observation that the nature of aliasing remains unchanged whether the under-sampled acquisition contains only low frequencies or includes high frequencies too. Here, the transformation needed to reconstruct the alias-free image from the aliased coil images is learnt, using acquisitions consisting of densely sampled low frequencies. Neural networks are made use of as machine learning tools to learn the transformation, in order to obtain the desired alias-free image for actual acquisitions containing sparsely sampled low as well as high frequencies. CRAUNN operates in the image domain, and does not require explicit coil sensitivity estimation. It is also independent of the sampling trajectory used, and could be applied to

---

*Corresponding Author

Email address: `neel.iam@gmail.com` (Neelam Sinha)

[1] Telephone: +91 80 25432753; Fax: +91 80 23600444

arbitrary trajectories as well. As a pilot trial, the technique is first applied to Cartesian trajectory-sampled data. Experiments performed using radial and spiral trajectories on real and synthetic data, illustrate the performance of the method. The reconstruction errors depend on the acceleration factor as well as the sampling trajectory. It is found that higher acceleration factors can be obtained when radial trajectories are used. Comparisons against existing techniques are presented. CRAUNN has been found to perform on par with the state-of-the-art techniques. Acceleration factors of up to 4, 6 and 4, are achieved in Cartesian, radial and spiral cases respectively.

Key words: Parallel Magnetic Resonance Imaging, under-sampling, non-Cartesian sampling, unaliasing, neural networks.

---

1. Introduction

Parallel MR Imaging is gaining popularity since it enables rapid imaging, leading to images with better spatio-temporal resolution. Typically, reduced data acquisition is carried out and prior knowledge of the coil sensitivities is used to obtain the desired image. Image reconstruction approaches are basically classified depending on whether it is carried out in image-domain or k-space or both. The quality of image reconstructed depends on the sampling trajectory, data reduction factor, as well as the reconstruction approach employed. Reduced data acquisitions along different sampling trajectories lead to aliasing of different nature, and hence the quality of image reconstruction depends on the complexities in unaliasing (generation of missing k-space points) for the trajectory employed. Some of the reconstruction strategies critically depend on the precise estimation of coil sensitivity. Problems of numerical instability might arise in the event of noisy acquisitions.

Pruessman et. al (1) proposed a method called "Sensitivity Encoding" (SENSE), first applied on Cartesian trajectories. Here, unaliasing is carried out in image domain, by framing the problem in linear algebraic framework. It is well-known that Cartesian regular under-sampling results in localized peaks in the point spread function (PSF), which enables one to compute the unfolding matrix in a straight-forward manner. Another advantage of Cartesian trajectory lies in the utilization of FFT for various operations, making the solution practical. Data acquisition along non-Cartesian trajectories (2) leads to reduced motion and flow-induced errors. Besides, it allows the start of data acquisition at the center of k-space along with the advantage of needing shorter scan paths to cover a given area, as compared to the Cartesian trajectories. However, in the case of under-sampled non-Cartesian trajectories, the PSF obtained is not localized and hence unaliasing is not straightforward. Besides, re-gridding is required to utilize the FFT algorithm, making the solution computationally demanding. The linear-algebraic framework used in (1) was extended to non-Cartesian trajectories by proposing an iterative solution using conjugate-gradient method, which is known as "Conjugate Gradient SENSE" (CG-SENSE) (3). Although this solution is widely used, it faces the problem of regularization in the event of poor SNR, leading to numerical instabilities. Many regularization techniques were reported (4) to counter problems of numerical instabilities, the most popular of them being Tikhonov (5) regularization scheme.

Another strategy for image reconstruction, that utilized projections on convex sets, called POCSENSE was proposed in (6). The advantage of this method lies in its capability to incorporate prior knowledge into the solution. This solution is also iterative, and unlike SENSE, poses the problem in a set-theoretic framework, rather than linear-algebraic, making it possible to incorporate non-linear constraints. Both of the above-mentioned methods face the drawback of needing a separate low-frequencies scan for estimation of coil sensitivities. However, this drawback is not seen in techniques such as (7), where Nyquist sampling of the low k-space is used to obtain blurred alias-free acquisitions. Regular Cartesian sampling schemes were modified to variable-density trajectories, with Nyquist sampling of the low k-space and sparse sampling of the outer k-space. The densely sampled low k-space was used to estimate the coil sensitivities, thus eliminating the need for a separate calibration scan. A technique utilizing B-splines (8) was recently proposed for reconstruction in parallel imaging. Here, coil-weighted aliased images are linearly combined to obtain the desired alias-free image. The reconstruction operator is determined from the images obtained using acquisitions containing only low frequencies. The same reconstruction operator is applied to images obtained using acquisitions containing the entire range of k-space frequencies. The coefficients that linearly combine, are expressed as a linear combination of B-splines. The reconstruction parameters are obtained by minimizing the error for the images obtained using acquisitions containing only low frequencies. This technique is restricted only to Cartesian sampled-data since it utilizes the localized behaviour of Cartesian PSF while arriving at the solution.

An entirely different approach to image reconstruction is to work in the k-space in order to generate the unacquired points. “Simultaneous acquisition of spatial harmonics" (SMASH) (9) was first proposed to generate the missing lines in k-space by linearly combining the coil sensitivity profiles. However, this method was not practically utilized because of the difficulties in the design of precise coil profiles. Most of the k-space based techniques proposed later utilize the acquired neighbouring points to generate the missing samples. The techniques differ in the method adopted to generate the combining co-efficients.The first k-space interpolation technique that linearly combined the acquired points within a local neighbourhood to generate the missing points, was called "Generalized Auto-calibrating Partially Parallel Acquisitions" (GRAPPA) (10). This method assumed uniformly-spaced acquisitions along Cartesian trajectories. However, low k-space was adequately sampled, with these lines being called "ACS" (Auto-calibration lines). The combining weights were determined using the ACS lines, and the same combining weights are used for the acquisitions of the entire k-space.

GRAPPA has been extended to handle non-Cartesian trajectories as well. Extension to radial sampling was proposed by laying out the acquired radial along a pseudo-Cartesian plane (11). The same idea was adapted for spiral acquisitions in (12). However, the drawback of this procedure was that it required a complete separate scan to determine the combining weights. This drawback was overcome in works that reported determination of the combining weights using Nyquist sampled low k-space (13) using dual-density spirals. In (14), interpolation kernels are separately generated for each sector that the k-space is divided into. Variations of GRAPPA like PARS (15) and 'Direct SENSE' (16) differ in the criterion for selection of the best neighbourhood. In methods like 'parallel image reconstruction based on successive convolution operations' (BOSCO) (17), convolution kernels are devised using low k-space, that are used to generate the missing points in the high k-space. In k-space based techniques the estimation of coil sensitivities is not very critical, and also they have the advantage that the processing takes place in the same domain as that of data acquisition. However, these methods are typically more computationally intensive than image-domain methods.

Hybrid methods such as "Sensitivity Profiles from an Array of Coils for Encoding and Reconstruction in Parallel" (SPACE-RIP) (18) that work in both image and k-space domains have also been explored. This method too requires estimation of coil sensitivities, which are used to partially encode the image. Reduced acquisition of k-space is carried out and images reconstructed.

Neural networks (NN) have been used in the recent past (19) to determine coil sensitivities at the spatial co-ordinates where the estimation otherwise carries no confidence. NN are used to extrapolate values at noisy points using the knowledge of the coil sensitivities at other points where the confidence in the values is higher. In (20), NNs are used to predict un-acquired k-space samples in the context of single-coil MR imaging.

The image reconstruction scheme proposed in this paper, "Composite image Reconstruction And Unaliasing using Neural Networks" (CRAUNN) works in the image domain. It is based on the observations about PSF obtained using acquisitions that contain only low frequencies and those that contain high frequencies too. Here, NN is used to learn the function that takes as input aliased coil images and outputs the corresponding unaliased image. Images obtained using low-frequency data are used in the training phase that determine the connecting weights in the network topology. The technique is applied to Cartesian, spiral and radial acquisitions of real and synthetic data.

The rest of the paper is organized as follows. Section 2 explains the CRAUNN approach. Section 3 discusses the data used, the results obtained, and comparisons with other standard techniques. Section 4 discusses the issues involved in the CRAUNN approach. The paper concludes with section 5.

2. Materials & Methods

2.1. Problem formulation for Cartesian sampling

In parallel MR scanners multiple receiver coils are used to improve image SNR. Images from the individual coils are separately reconstructed and combined to yield a composite image, which serves as a benchmark for quality comparisons with reduced data parallel imaging reconstruction schemes. The problem formulation for Cartesian sampling, discussed here, can be extended to non-Cartesian cases too.

The notations used here are taken from the paper (8). The composite image (here, root-sum-of-squares), when there is no acceleration, is assumed to be the true image. For accelerated Cartesian data acquisition, where each coil under-samples the data, the image acquired from the lth coil, S_l is given as,

$$S_l(x, y) = C_l(x, y)S(x, y) \tag{1}$$

where C_l is the complex sensitivity of the lth coil, and S is the true image.

It is well-known that sparse sampling in k-space causes aliasing in image domain. In the event of rectangular uniform under-sampling by factor M where N_y is the maximum number of phase encodes possible corresponding to the full unreduced FOV, the aliased image obtained at the lth coil, S_l^A is given by,

$$S_l^A(x,y) = \sum_{m=0}^{M-1} S_l(x, y + m\frac{N_y}{M}) \tag{2}$$

Hence,

$$S_l^A(x,y) = \sum_{m=0}^{M-1} C_l(x, y + m\frac{N_y}{M}) S(x, y + m\frac{N_y}{M}) \tag{3}$$

In the CRAUNN approach, the image reconstruction operator is assumed to be a function of the aliased coil images, processed pixel-wise. The reconstruction function, $\mathbf{F}$, to estimate the composite alias-free image S, is given as:

$$S(x,y) = \mathbf{F}\left(S_l^A(x,y)\right) \tag{4}$$

where, $l = 1, 2, \cdots, L$. The function is allowed to be arbitrary in form and complexity, and is determined using neural networks. Unaliasing and combining of coil images to generate the composite image are accomplished together by the neural network, without explicitly requiring the coil sensitivity estimation.

2.2. PSF Observations : Basis of CRAUNN

The proposed method, CRAUNN, is based on the observation that for a fixed under-sampling factor, the nature of the PSF remains the same, irrespective of whether the regularly under-sampled acquisition contains only low frequencies or both high and low frequencies. As is well-known in the case of Cartesian sampling (see Fig. 1(a-b)), for a fixed under-sampling factor, the PSF obtained for a low-frequency acquisition peaks at precisely the same points as the PSF for an acquisition containing both low and high frequencies. In the case of low-frequency acquisition, the peaks get smeared, indicating blurring. Similar observations can be made from Figs. 1(c-f), which show the magnitudes of PSFs for spiral and radial acquisitions for the under-sampling factor of 2. The extent of aliasing is shown by the brightness of the regions seen in the figures. Here, the PSFs are not localized unlike the Cartesian case and hence unaliasing is not straightforward. In the case of spiral sampling, accelerated scans mean utilization of lesser number of spiral interleaves. As the spacing between two consecutive interleaves increases, the concentric circles seen in the PSF get closer leading to greater aliasing. In the case of radial sampling, acceleration implies utilization of lesser number of radial projections. As the spacing between two consecutive radial projections increases, the streaking artifacts increase. Radial PSF offers an inherent advantage over spiral PSF since the aliasing artifacts occur away from the center.

2.3. Overview of CRAUNN reconstruction

Figure 2 gives an overview of the proposed reconstruction technique. This method needs an unaliased dataset of low k-space acquisition. The neural network architecture used here is a single hidden layer feed-forward network with radial basis functions. The input layer consists of 18 nodes, while the output layer is made of a single node. The hidden layer has 98 nodes. The details of the neural network parameters can be found in the appendix. The complex pixel intensities of the coil images and their spatial co-ordinates

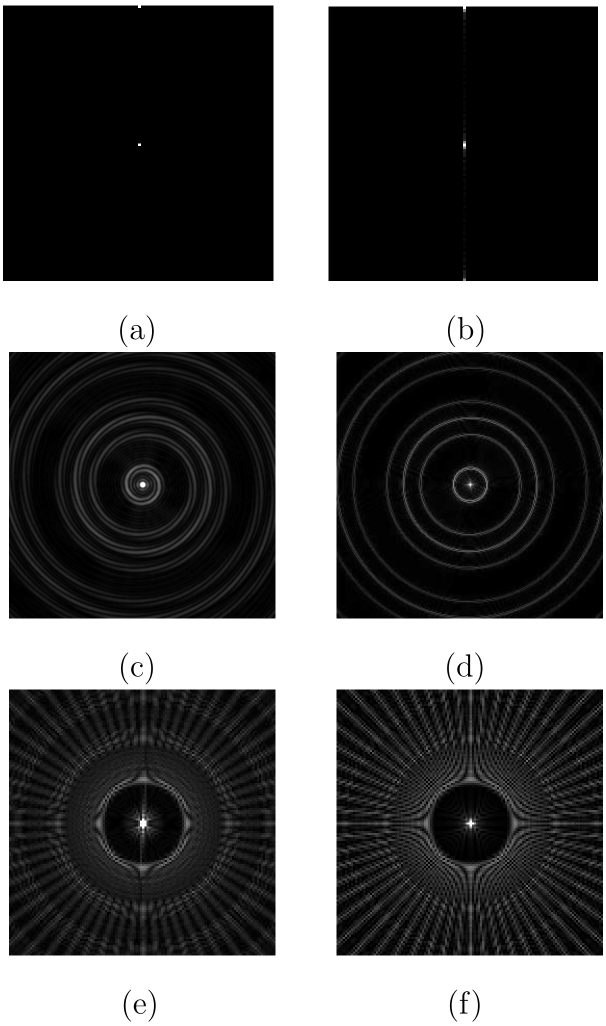

(a) (b)

(c) (d)

(e) (f)

Figure 1: Illustration that the nature of aliasing does not depend on the extent of frequency content in the acquisition. The figures show the PSF obtained on under-sampling different trajectories. From top to bottom, the panels correspond to Cartesian, spiral and radial acquisitions, respectively. Figures on the left side of each panel show the PSF for low frequencies only, whereas those on the right display the PSF for both low and high frequencies.

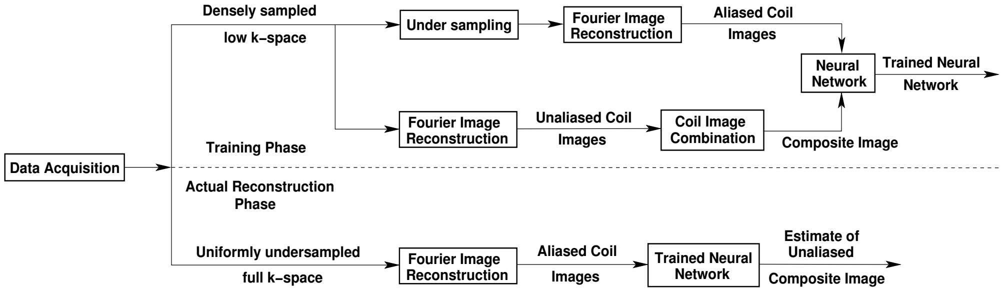

Figure 2: Image reconstruction by CRAUNN: The acquired data is selectively used to obtain different images at different stages of the image reconstruction (The top leg of the block diagram represents the training phase, while the bottom leg represents the actual reconstruction phase)

together form the feature vector. The system works in 2 phases, namely training (learning) and reconstruction.

2.3.1. Images for learning and reconstruction

Figure 2 explains how the acquired data is selectively utilized to obtain images for different purposes in the course of image reconstruction using the CRAUNN approach.

- Alias-free Images containing only low frequencies : It is well-known that alias-free acquisitions can be obtained by considering k-samples within low k-space where the sampling density satisfies Nyquist requirements. While Cartesian sampling schemes are modified to variable-density trajectories, non-Cartesian sampling trajectories may not need modifying since they inherently over-sample low k-space. In the case of spiral sampling, variable density spirals are used, such that a central disk of radius $k_{max}/10$ is sampled at Nyquist rate. This densely sampled disk is used to obtain alias-free acquisitions. However, in radial sampling, variable density sampling is not possible. Hence a separate alias-free low-frequency acquisition scan is required in order to obtain blurred alias-free coil images. The alias-free coil images are combined to obtain the composite alias-free blurred version of the true image. Here, the composite image is taken as the root-sum-of-squares combination.

- Aliased Coil Images containing only low frequencies : During training, the aliased coil images containing only low frequencies form the input to the system, while the corresponding alias-free image obtained from the preceding section forms the target of the system. Low k-space samples that affect under-sampling by the desired acceleration factor are retained, thereby generating aliased coil images with low frequencies alone. Now aliased coil images and the corresponding true image containing the same set of low k-space frequencies are obtained, which is what is required in the training phase.
- Aliased Coil Images containing both low and high frequencies : These images are used in the reconstruction phase. The aliased coil images containing both low and high frequencies are obtained by considering the uniformly under-sampled k-space. The appropriate samples in the low k-space are ignored in order to introduce aliasing by the required acceleration factor. Features from these aliased coil images are input to the configured neural network. The output is the estimate (reconstruction) of the corresponding alias-free image.

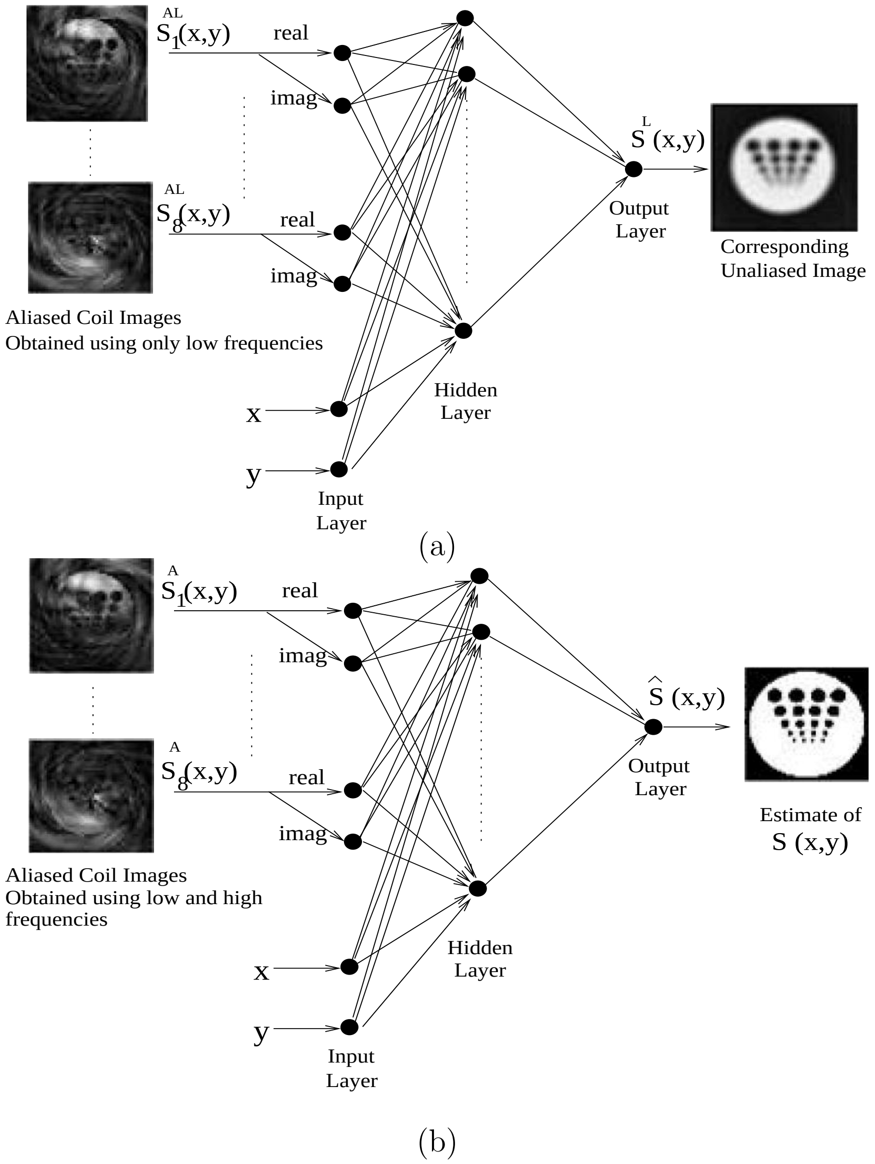

Figure 3: Training and reconstruction phases of CRAUNN.

(a) Training phase. The inputs are the intensities of corresponding pixels from all the aliased coil images, as well as the co-ordinates of the pixel, while the output is the corresponding pixel intensity of the alias-free composite image; Images here contain only low frequencies. (b) Reconstruction phase. Inputs are the aliased coil images containing both low and high frequencies uniformly under-sampled. The output is the estimate of the desired image.

2.4. Training and Reconstruction phases

CRAUNN reconstruction works in two phases: Training phase and Reconstruction phase, as shown in Figs. 3(a) and (b), respectively.

In the training phase, the system learns the transformation that takes as input, aliased coil images and outputs the corresponding true alias-free composite image. In the reconstruction phase, the transformation thus learned in the training phase from the fully sampled central k-space lines is used. In this phase, the images are constructed using both low and high frequencies, uniformly under-sampled. Here the configured system is fed aliased coil images, and outputs the estimate of the desired alias-free, composite image. In this phase, only the low k-space data (the ACS data acquired at Nyquist rate) is used. At the end of this phase, the interconnecting weights among the nodes in the various layers are frozen, and the system is said to be configured for the image reconstruction.

In the reconstruction phase, the transformation thus learned in the training phase from the fully sampled central k-space lines is used. In this phase, the images are constructed using both low and high frequencies, uniformly under-sampled. Here the configured system is fed aliased coil images, and outputs the estimate of the desired alias-free, composite image.

3. Results

All simulations are carried out in MATLAB. CRAUNN is applied to Cartesian, spiral and radial data. Results are shown for different categories of data in order to illustrate the performance of the method: actual acquisitions of data from human subjects as well as real phantom, data computed from simulated phantoms, actual and simulated Cartesian acquisitions interpolated along spiral/radial trajectories to simulate spiral/radial data. For all the non-Cartesian cases, re-gridding on a 2X grid is performed as in (21) using a Kaiser-Bessel window of width 2.5. Errors in image reconstruction are quantified using error images as well as by comparing scan lines that run through the images. Besides, ‘Structural similarity index measure’ (SSIM) (22) is used to assess the quality of image reconstruction. SSIM is widely used by the image/video processing community in order to evaluate degradations in image/video reconstruction, based on structural similarities with the original. This is similar to perceptual difference model, a popular tool for quantitative evaluation of MR image quality (23), which also utilizes correlation with human rating. SSIM is a full-reference metric. The technique needs a gold standard image with respect to which the similarity of the test image is determined. In our work, the gold standard used is the image obtained using un-accelerated scans, while the test image is the reconstruction obtained from reduced data sets using the proposed technique. The SSIM code available at the website http://www.ece.uwaterloo.ca/˜z70wang/research/ssim has been used for evaluations.

3.1. Reconstructions from Cartesian data :

A real brain data set (8-coil data) utilized in (24), available on the website http://www.ece.tamu.edu/˜mrsl/JIMJI_TAMU/ pulsarweb/index.htm is used for the study. The data matrix is of size 256 × 256. The central 32 lines are sampled at Nyquist rate, while the remaining k-space is sparsely sampled, depending on the down-sampling factor. Figure 5 compares the reconstructed and the corresponding error images, for a downsampling factor of 4, for the brain image shown in Figure 4. The same sparsely sampled data is used for reconstruction using the standard parallel imaging techniques, SENSE and GRAPPA, for down-sampling by 4 and 32 Nyquist sampled low k-space lines. The SENSE and GRAPPA reconstructions have been obtained using codes available at http://www.ece.tamu.edu/~mrsl/JIMJI_TAMU/ pulsar-web/index.htm.

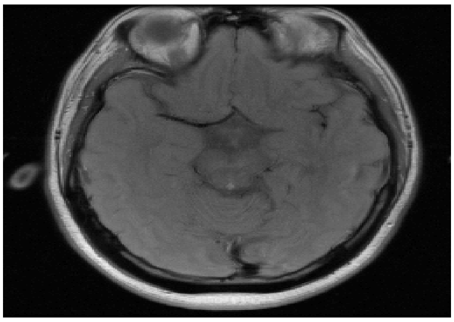

Figure 4: Real data : Original image of the brain data used for the study.

3.2. Reconstructions from spiral data :

Phantom data is obtained using a 8-channel head coil and a gradient echo spiral pulse sequence (16 interleaves, 3096 samples per interleaf) on a GE 1.5 T Excite scanner. The spiral trajectory desired is such that the lower k-space up to $k_{max}/10$ is sampled at Nyquist rate, while fewer interleaves are used among higher frequencies. All the spiral data sets are density compensated and re-gridded to Fourier-reconstruct the corresponding images. All the Fourier-reconstructed images are then cropped to a 256 × 256 grid. To simulate accelerated scans, a subset of spiral interleaves are set to zero, depending on the acceleration factor. For example, for an acceleration factor

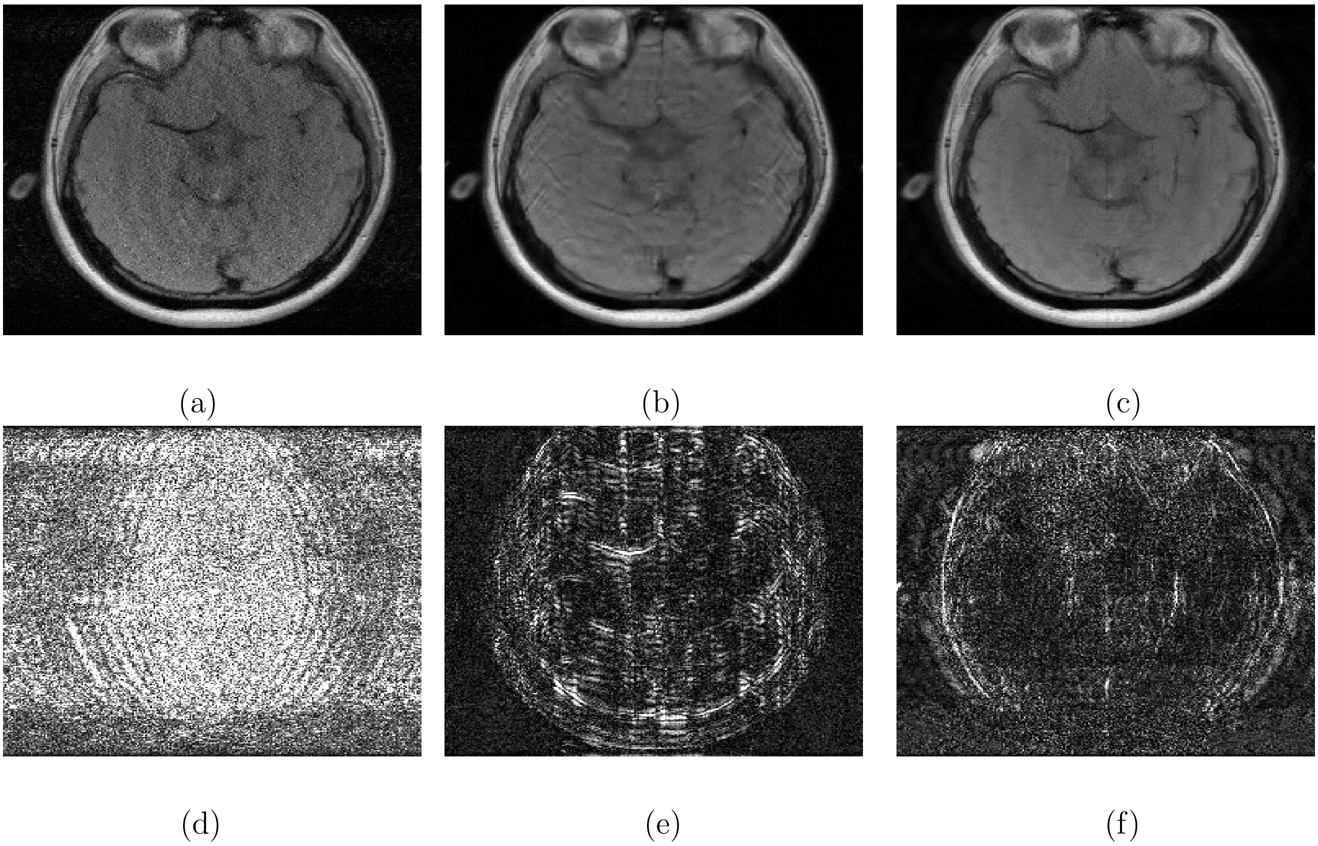

Figure 5: Performance on the real brain data image shown in Fig. 4 for Cartesian undersampling by 4. Top Panel : Comparison of images reconstructed by (a) SENSE (b) GRAPPA (c) CRAUNN (color scale : 0 to 255). Bottom Panel : Comparison of error images. (d) SENSE (e) GRAPPA (f) CRAUNN (color scale : 0 to 34)

of 2, every alternate spiral interleave is set to zero. The well-known CG-SENSE is also used to reconstruct the same data. We have utilized the code for CG-SENSE applicable to Cartesian trajectories available at the website http://www.nmr.mgh.harvard.edu/~fhlin/tool_sense.htm. For image reconstruction using data sampled along spiral and radial trajectories, routines for density compensation and re-gridding had to be added to the existing code. The iterative CG-SENSE reconstruction is considered to have converged using the delta-convergence check (3). The reconstructed and error images are shown in Fig. 6.

The rectilinearly acquired brain data utilized in the Cartesian case is now spirally re-sampled with 24 interleaves, with 4015 points in each interleaf. To simulate accelerated scans, this data is undersampled by the appropriate factor. The reconstructions obtained using both CRAUNN and CG-SENSE are compared in Fig. 7. The spirally re-sampled data will show up artifacts due to motion, susceptibility, etc. different from data acquired along spiral trajectories. A simulated standard phantom, used in non-Cartesian MR studies (25), is also used to assess the performance of the CRAUNN method. The reconstruction parameters remained the same as in the preceding data set. The results obtained and the comparison with those of CG-SENSE are shown in Fig. 8.

3.3. Image reconstructions from radial data :

For the radial case, a synthetic phantom is created with 180 projections each with 128 points. The phantom is multiplied with the 8-coil complex sensitivity data available on http://www.ece.tamu.edu/~mrsl/JIMJI_TAMU /pulsarweb/index.htm, and transformed to k-space in order to simulate 8-

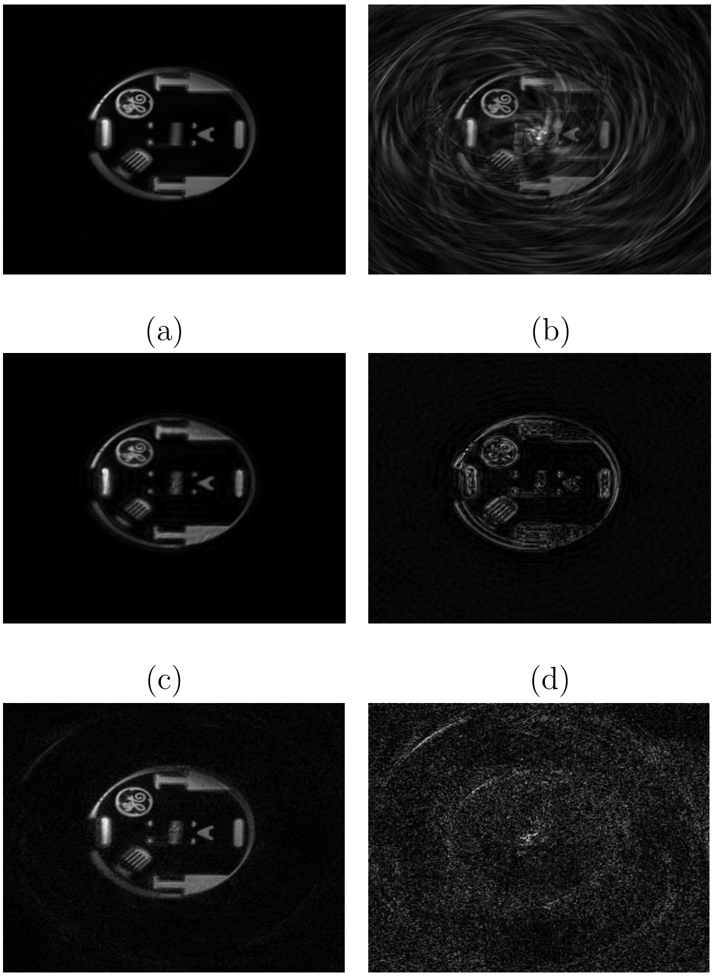

(a) (b) (c) (d) (e) (f)

Figure 6: Performance comparison on a real phantom data set for spiral under-sampling by 4. (a) True image (16 spirals) [0-255]. (b) Direct reconstruction of under-sampled data [0-255]. (c) Reconstruction with CRAUNN [0-255]. (d) Corresponding error image [0-60]. (e) Reconstruction using CG-SENSE [0-255]. (f) Corresponding error image [0-51].

channel parallel MR data. Complex noise is added to the obtained k-space with an SNR of 10 dB, in order to simulate conditions of real acquisition. Ac-

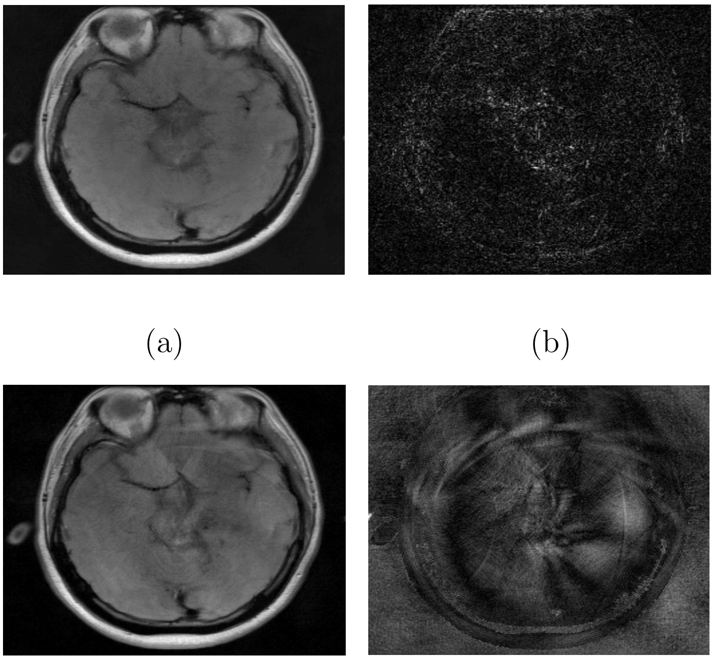

(a) (b)

(c) (d)

Figure 7: Comparison of reconstructions of real brain data shown in Fig. 4 for spiral under-sampling by 4. (a) Reconstruction with CRAUNN [0-255]. (b) Corresponding Error image [0-25.5]. (c) Reconstruction using CG-SENSE [0-255]. (d) Corresponding Error image [0-46].

celerated data is obtained by ignoring the appropriate number of radial projections. All the radial data sets are density compensated and re-gridded to Fourier-reconstruct the corresponding images. All the Fourier-reconstructed images are then cropped to a 128 × 128 grid. Unlike the Cartesian and spiral cases, reconstruction of accelerated radial data requires a pilot scan with unaccelerated acquisition within a certain k-space radius. For the simulations carried out, it is assumed that all samples till the frequency $k_{max}/10$ are available along all the projections . These low frequency acquisitions are

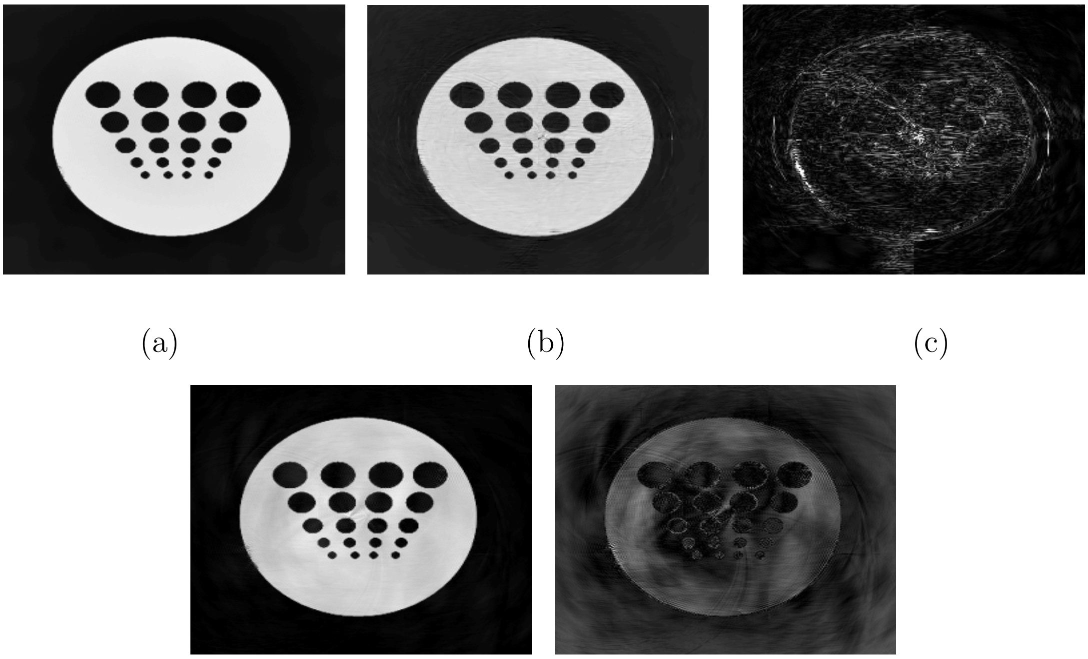

(a) (b) (c)

(d) (e)

Figure 8: Comparison of reconstructions of a simulated data set for spiral under-sampling by 4. (a) Original image [0-255]. (b) Reconstruction with CRAUNN [0-255]. (c) Corresponding error image [0-92]. (d) Reconstruction using CG-SENSE [0-255]. (e) Corresponding error image [0-92].

used for the training phase. For the actual reconstruction, accelerated data sets are used. The reconstructed and error images using both CRAUNN and CG-SENSE are shown in Fig. 9.

In addition, the real data used for Cartesian case, is again re-sampled radially (180 projections, 385 points) in k-space. Because of this, the results obtained on this data must be treated only as proof of principle. After density compensation and re-gridding, all Fourier-reconstructed images are cropped to a 256×256 grid in this case. For comparison, reconstruction using under-sampled data (x6) is performed using both CRAUNN as well as CG-SENSE. The reconstructions obtained using CRAUNN as well as those obtained using CG-SENSE are shown in Fig. 10.

4. Discussion

The reconstruction method proposed in this paper, CRAUNN, makes no assumptions about the nature of the sampling trajectory and hence can be generalized to any arbitrary trajectory. Cartesian data acquisition is a simple, tractable case and hence was attempted, first as a proof of concept of the CRAUNN approach. Encouraging results obtained here enabled us to proceed further to the non-Cartesian cases. The function that processes the aliased coil images to yield the alias-free true image, is estimated with no assumptions of form or complexity. The only underlying assumption is that the transformation that holds for acquisitions containing low frequencies alone also holds good for acquisitions that contain high and low frequencies, as seen from the observations made using the PSF images. The fact that the network is solely trained by the same image, leads to fewer artifacts than could have occurred if features from other images would be learnt. Besides, explicit evaluation of coil sensitivities is not required, which is an advantage, compared to existing methods like CG-SENSE. Unregularized SENSE is utilized to justify the comparison since CRAUNN does not incorporate any noise-related information.

The results for Cartesian acquisition are shown in Fig. 5. It is seen that the reconstruction obtained using SENSE clearly preserves the structures, but loses out on account of allowing bright replicates. The replica-

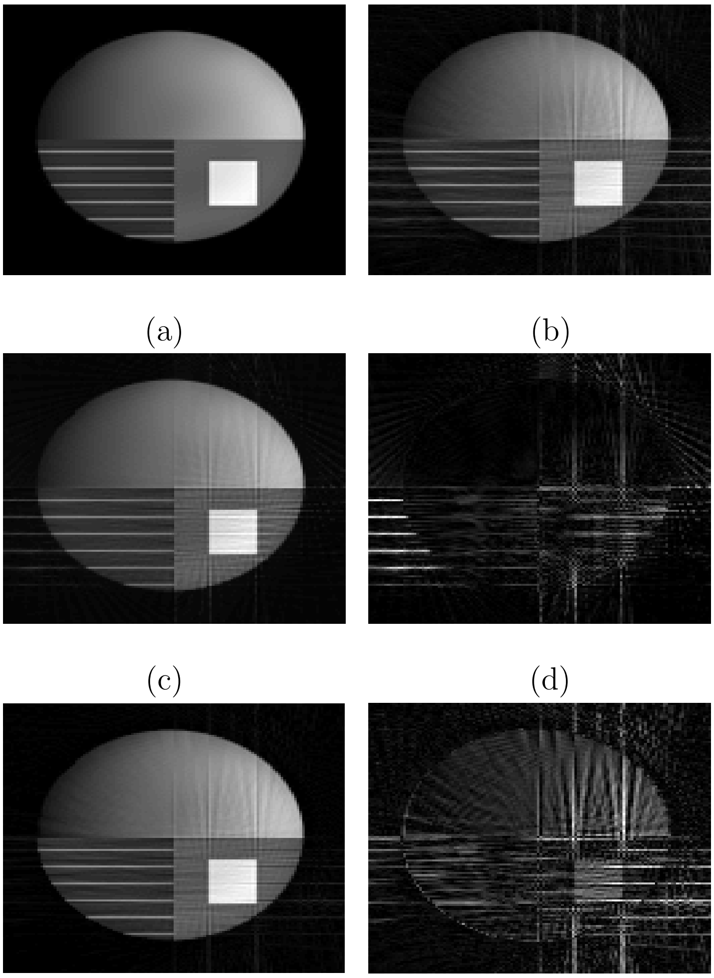
(a) (b)
(c) (d)
(e) (f)

Figure 9: Comparison of reconstructions of a simulated phantom using radial under-sampling by 6. (a) Simulated phantom reconstructed using 180 radials [0-255]. (b) Direct reconstruction using data under-sampled by 6 [0-255]. (c) Image reconstructed with CRAUNN [0-255]. (d) Corresponding error image [0-50]. (e) Image reconstructed using CG-SENSE [0-255]. (f) Corresponding error image [0-55].

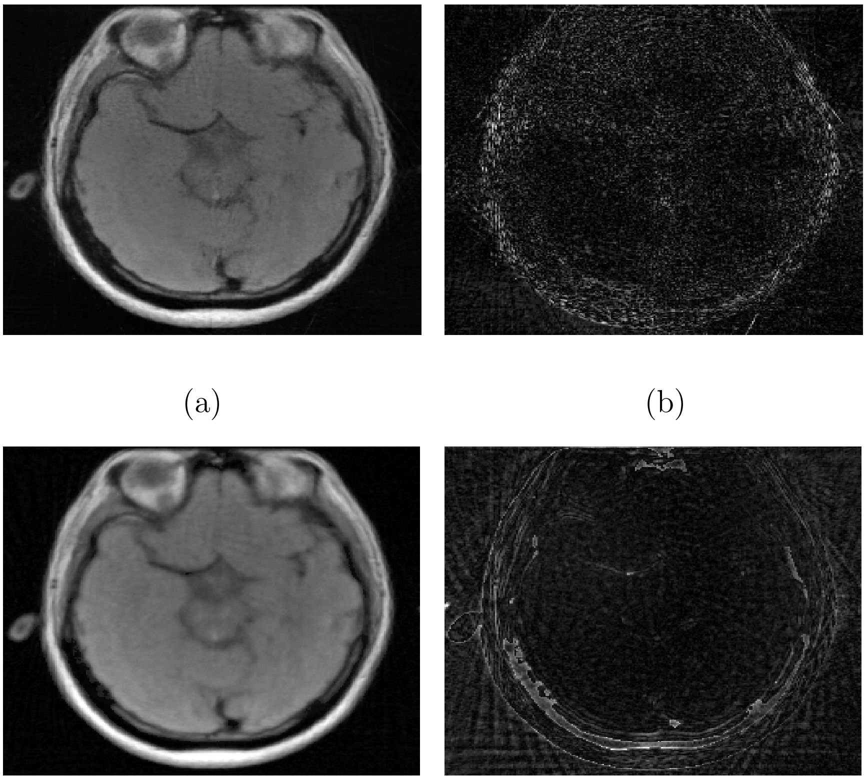

(a) (b)

(c) (d)

Figure 10: Performance comparison of CRAUNN and CG-SENSE on brain data shown in Fig. 4 using radial under-sampling by 6. (a) Image reconstructed using CRAUNN [0-255]. (b) Corresponding Error image [0-38]. (c) Image reconstructed using CG-SENSE [0-255]. (d) Corresponding Error image [0-46].

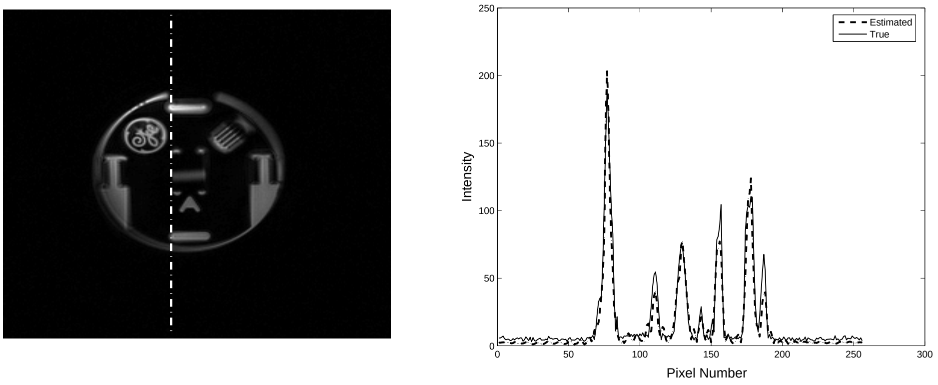

(a) (b)

Figure 11: Comparison of a scan line through the original and reconstructed images using CRAUNN for spiral sampling (under-sampled by 4) for the data used in Fig. 6.

tion of larger structures stands out in the reconstruction. Reconstruction using CRAUNN and GRAPPA are comparable. The output obtained using GRAPPA is visibly textured on both sides of what should have been a homogeneous-looking region. CRAUNN output looks relatively clearer, but also results in an artifact seen in the image off-center to the right, as a dark streak.

In spiral and radial trajectories, the center of the k-space is adequately sampled, and hence the direct reconstruction without any intermediate processing of the sparsely acquired data also preserves the broader details of the image. However, the differences in reconstruction appear more prominently in the finer details. Comparison of the profile lines for the reconstructed images for spiral and radial cases are shown in Figs. 11 and 12 respectively. The comparison of the finer image details in the reconstructed images for spiral and radial cases are shown in Figs. 13 and 14, respectively.

In the results obtained for the spirally re-sampled brain image (See Fig.

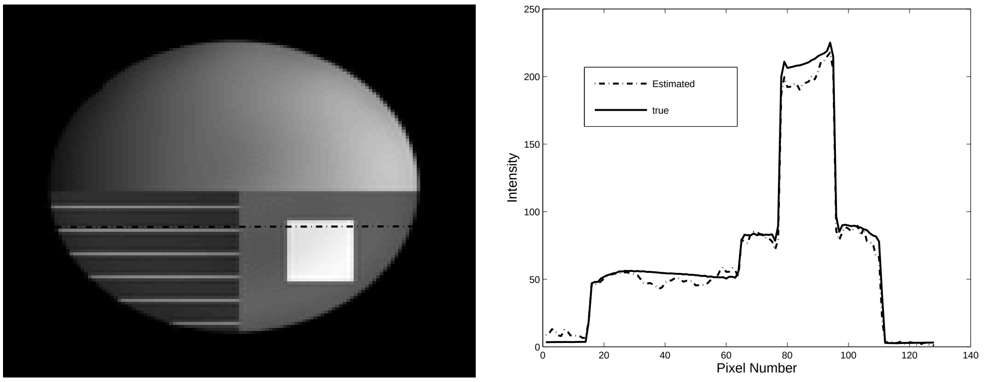

(a) (b)

Figure 12: Comparison of a scan line through the original and reconstructed images using CRAUNN for radial sampling (under-sampled by 6) for the data used in Fig. 9.

7) , the reconstructions obtained using CRAUNN and CG-SENSE are compared. The error images show the residual aliasing in the image obtained using CG-SENSE, which is not seen in the image obtained using CRAUNN. In the case of radial sampling, (See Fig. 10), greater acceleration factors are possible since the nature of aliasing leads to artifacts away from the center of the FOV. Most of the artifacts encountered here are mainly the streaking artifacts towards the image corners.

The comparison of the SSIM indices for the phantom image reconstructed using CG-SENSE and CRAUNN are shown in Fig. 15. The scale of the SSIM indices range from 0 to 1, where 0 shows very poor similarity to the original image, while 1 shows the best similarity. It can be seen that CRAUNN results in greater similarity to the reference image, as the SSIM indices show greater brightness than the one obtained using CG-SENSE. However, there are isolated spots such as the centre of the FOV and part of the right extreme of the FOV, where CG-SENSE has better similarity with the original.

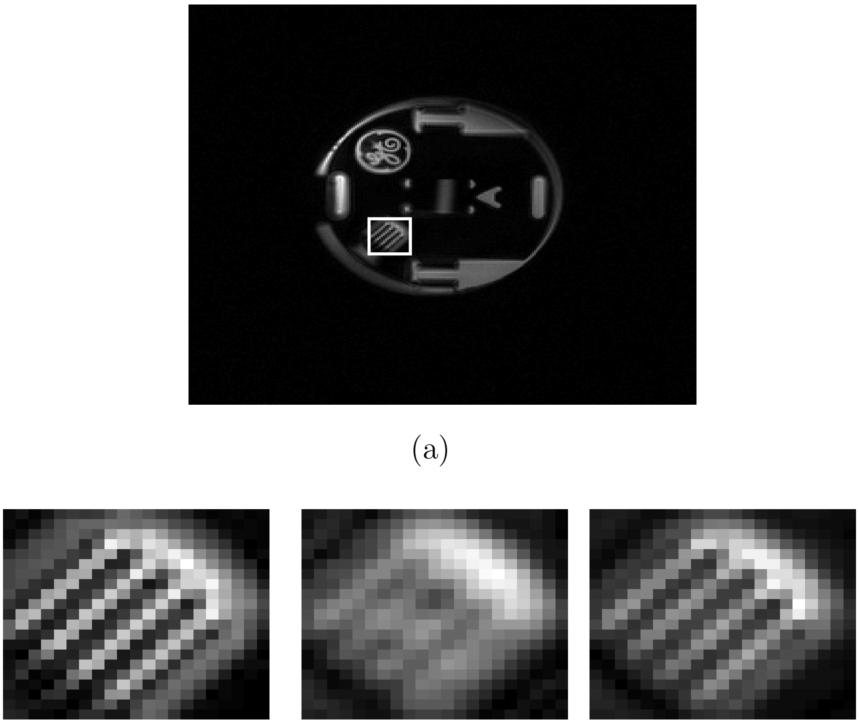

(a)

(b) (c) (d)

Figure 13: Comparison of details in the reconstructed images using the data shown in Fig. 6. (a) Original Phantom image. The region being observed for details is a comb-like structure marked by a rectangle. Spiral data used is under-sampled by 4. (b) Comb in the original image. (c) Comb in the direct reconstruction. (d) Comb in the reconstruction using CRAUNN.

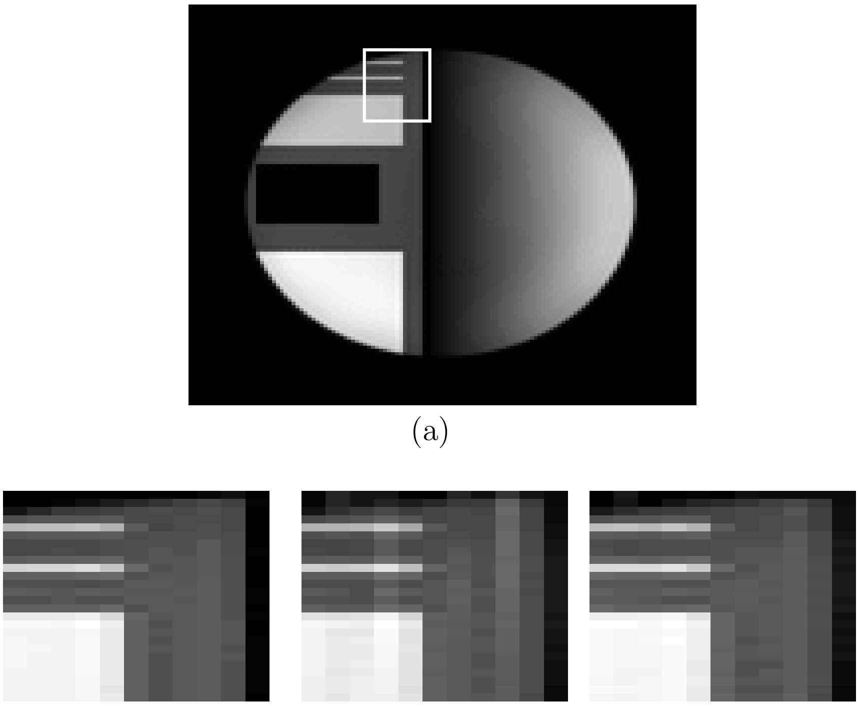

(a)

(b) (c) (d)

Figure 14: Comparison of details in the reconstructed images of a synthetic phantom. (a) Original Phantom image. The region being observed for details is marked by a rectangle. Radial data used is under-sampled by 6. (b) Detail in the original image. (c) Detail in the direct reconstruction. (d) Detail in the reconstruction using CRAUNN.

An experiment was carried out where the low k-space area that is Nyquist sampled, is reduced to half the size. Figure 16 shows that the resulting image is blurred in this case. This is because using very low frequency acquisitions for training the neural network, teaches the network to yield smoothened images. The fine features in the image do not get registered with the network, thus leading to blurring artifacts in the reconstructed image. Although the experiment was carried out on spirally sampled data, the observations can

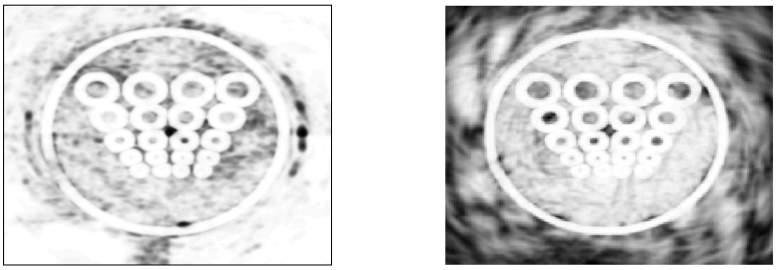

(a) (b)

Figure 15: : Comparison of SSIM indices of the reconstructions of the phantom shown in Fig. 8(a). (a) SSIM indices of CRAUNN reconstruction [0-1]. (b) SSIM indices of CG-SENSE reconstruction [0-1]. Higher intensities denote better similarity with the original image.

be extended to Cartesian and radial data too.

The time taken by CRAUNN to reconstruct images of size 256 × 256, on a pentium 2.6 GHz processor (with 1 GB RAM) using MATLAB codes, is about 5 minutes. On the other hand, CG-SENSE is quicker and takes less than 2 minutes on the same machine for images of the same size.

The neural network topology, learning parameters and feature vectors used, have been the same all through, for the different sampling trajectories used. Since the number of feature vectors is equal to the number of pixels in the image, each feature vector being independent of all others, the CRAUNN approach is parallelizable across pixels, and can be made faster.

The drawback of the CRAUNN approach is that it is not possible to compute the confidence level of the estimate of pixel intensities, unlike the case of SENSE. Further, it is difficult to predict the nature of artifacts that might appear in the reconstructed images. The training phase needs about hundred iterations to converge to an error of $(1/100)^{th}$ of the maximum intensity. For larger acceleration factors, the reconstruction errors are larger. One of

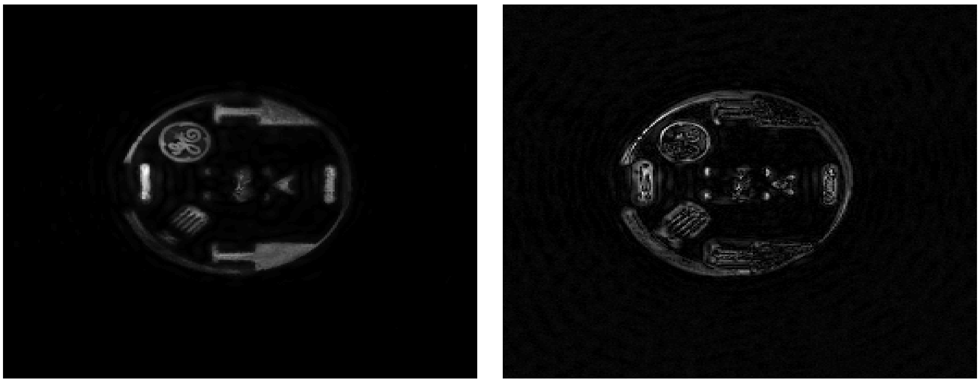

(a) (b)

Figure 16: Reconstruction using reduced low k-space acquisition for training (Spiral data used in Fig. 6 undersampled by 4). (a) Reconstructed Image [0-255]. (b) Corresponding Error image [0-70].

the reasons is that the training error itself saturates at a marginally higher value for larger acceleration factors. Fig.17 shows the typical behaviour of the training error observed with different acceleration factors. As seen in the plot, the training error at acceleration factor 2 saturates at a slightly lower value compared to the training error at acceleration factor 4.

5. Conclusion

For parallel magnetic resonance imaging, a neural network framework is proposed that reconstructs composite images and performs unaliasing of coil images. Here, the observations about the nature of artifacts being similar irrespective of whether the acquisition contains low frequencies alone, or include higher frequencies too, is exploited. Images obtained using low k-space frequencies are used to learn the model needed for image reconstructions

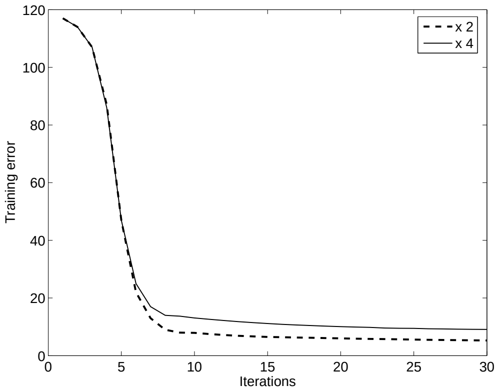

Figure 17: Typical plot of neural network training error (Y-axis) vs. number of iterations (X-axis), for different acceleration factors.

using the entire range of k-space frequencies. The CRAUNN approach is demonstrated to work for spiral and radial trajectories. CRAUNN can be applied to arbitrary trajectories in general. No assumptions are made about the transformation that is sought. From our experiments, we find that acceleration factors up to 6 are achieved with radial trajectories, while Cartesian and spiral trajectories result in acceleration factors up to 4.

6. Acknowledgements

We acknowledge the group that has made available valuable resources on the website http://www.nmr.mgh.harvard.edu/˜fhlin/tool_sense.htm. We have utilized the code for CG-SENSE applicable to Cartesian trajectories from this website. For image reconstruction using data sampled along spiral and radial trajectories, routines for density compensation and re-gridding had to be added to the existing code.

We also acknowledge the efforts of the group for sharing their valuable resources on the website http://www.ece.tamu.edu/~mrsl/JIMJI_TAMU/ pulsarweb/index.htm. We have utilized the structural brain data and codes for SENSE and GRAPPA from the resources made available at this website.

We acknowledge the efforts of the group that put up their publications and codes on the website http://www.ece.uwaterloo.ca/~z70wang/research/ssim. We have utilized the SSIM code made available at their website.

7. Appendix

Neural networks have emerged as a powerful mathematical tool for solving various problems like pattern classification and medical imaging due to their suitability for mapping complex characteristics, and learning. Of the many neural network architectures proposed, single hidden layer feed-forward network with sigmoidal or radial basis function are found to be effective for solving a number of real-world problems. The free parameters of the network are learned from the given training samples using gradient descent algorithm.

7.1. Multi-layer Perceptron (MLP) Network

A typical MLP network consists of three or more layers of processing nodes (neurons): an input layer that receives external inputs, one or more hidden layers, and an output layer which produces the target outputs. Using universal approximation property, one can say that the single layer feed-forward network with sufficient number of hidden neurons m can approximate any function to any arbitrary level of accuracy. It implies that for bounded inputs to the network there exist optimal weights (not necessarily unique) to approximate the function. Hence, in our study, we also use single hidden layer network to approximate the functional relationship between the aliased coil images and the true image. Let $\mathbf{U}$ be the n-dimensional features ($\mathbf{U} \in \Re^n$) input to the network. At the hidden layer, this input vector is transformed to an m-dimensional ($m > n$) intermediate vector $\mathbf{V}$, by the hidden neurons whose activation function is commonly chosen as the bipolar sigmoid function, defined as

$$f(t) = \frac{1.0 - exp(-t)}{1.0 + exp(-t)} \tag{5}$$

The intermediate vector ($\mathbf{V}$) comprises of elements v_i computed as

$$v_i \quad = \quad f\left(\sum_{j=1}^{n} w_{ij} u_j\right) \qquad i = 1, 2, \cdots, m \tag{6}$$

where w_{ij} is the weight connection between the jth input neuron and ith hidden neuron. The output ($\hat{P}$) of the MLP network with m hidden neurons and a single output neuron is given by:

$$\hat{P} = f\left(\sum_{j=1}^{m} \tilde{w}_j v_j\right) \tag{7}$$

where $\tilde{w}_j$ is the weight connection between the jth hidden neuron and the output neuron.

7.2. Back Propagation Learning Algorithm

Back Propagation (BP) is one of the simplest and most general methods for the supervised training of MLP (26). The basic BP algorithm works as follows:

1. Initialize all the connection weights ($\mathbf{W}$ and $\tilde{\mathbf{W}}$) with small random values from a pseudorandom sequence generator.
2. Compute the network output for the given input features $\mathbf{U}$.
3. Let P be the target output for a given input $\mathbf{U}$. Calculate the deviation of network output $\hat{P}$ from the target value

$$E \quad = \quad \frac{1}{2} \sum_{\forall \mathbf{U}} \left(\hat{P} - P\right)^2 \tag{8}$$

4. Compute the negative gradient of error to update the network weights

$$\Delta w_{ij} \quad = \quad -\frac{\partial E}{\partial w_{ij}} \tag{9}$$

5. Update the weights using negative gradient of error E until convergence of weights, i.e., the present error E must be equal to or smaller than the prescribed value.

The criterion for convergence is set as

$$|E| \quad <= \delta \tag{10}$$

Here δ is chosen to be 10^{-3}.

7.3. Architecture of the neural network

The neural network architecture used here is a single hidden layer feed-forward network with radial basis functions. The input layer consists of 18 nodes (since the input feature vector is made of 18 components), while the output layer consists of a single node (since the output is real). The hidden layer consists of 98 nodes, based on the standard procedure carried out for determination of the number of hidden neurons. The neural network is designed to output a real number for every feature vector presented. Hence the number of nodes at the output layer should be 1.

7.3.1. Neural network parameters

The activation functions used are all sigmoidal functions. The learning rate is chosen such that the error between iterations reduces rapidly enough for quicker convergence, but does not get trapped at local minima. Experimentally it was found that setting the learning rate below 10^{-6} reduced error between iterations too slowly, while setting the learning rate greater than 10^{-6} resulted in oscillatory behavior between iterations. Hence, the learning rate was set to 10^{-6}. The choice of the number of hidden neurons decides how smoothly the target function can be modeled. In practical situations, the appropriate number is chosen across several trials, where initialization is done with a fixed number greater than at least four times the length of the feature vector, as a rule of thumb. As seen in the plot in Fig. 18, the number is increased gradually and the corresponding training error is observed. The training error hits a minimum at a point, and thereafter gradually increases. The number of hidden neurons is clamped at the value where the training error is measured to be the least. Here it turns out to be 98.

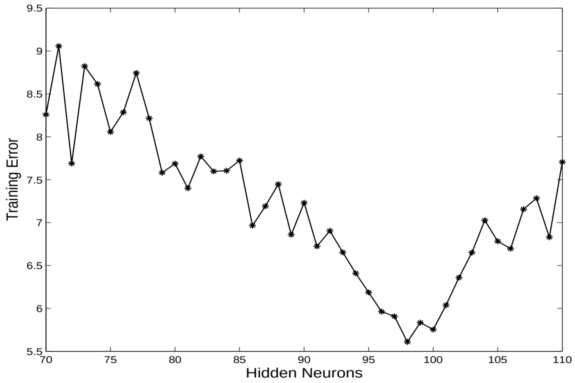

Figure 18: Plot showing variation of training error against number of hidden neurons

7.3.2. Input Features

The input layer of the neural network is fed with features extracted from the aliased coil images. The features used here are the complex pixel intensities of the coil images and their spatial co-ordinates. Here 8-coil data is used and hence 8 complex coil images are available. At a fixed location (x,y), for all the 8 coils, 8 complex numbers are obtained, which are split into their real and imaginary parts (2 x 8 = 16). The spatial co-ordinates ((x co-ordinate, y co-ordinate) = 2) for that location, are concatenated, making the feature vector length 18. It must be noted that inclusion of spatial co-ordinates in the feature vector, facilitates the transformation to be spatially varying.

7.3.3. CRAUNN algorithm

Training phase :

- The input feature vector $\mathbf{U_t}$ for the location (x,y) derived from the aliased coil images of low-frequency acquisitions, $S_1^{AL}, \dots S_8^{AL}$, given by

$$\mathbf{U_t} = \left[Re(S_1^{AL}(x,y)), Im(S_1^{AL}(x,y)), \dots Re(S_8^{AL}(x,y)), Im(S_8^{AL}(x,y)), x, y\right] \tag{11}$$

- The output of the hidden layer, a vector of 98-dimensions ($\mathbf{V_t}$) comprises of elements computed as

$$v_{ti} \;=\; f\left(\sum_{j=1}^{18} w_{ij} u_{tj}\right) \quad i = 1, 2, \cdots, 98 \tag{12}$$

- At the output layer, the output $\hat{P}$ is computed as

$$\hat{P} = f\left(\sum_{j=1}^{98} \tilde{w}_j v_{tj}\right) \tag{13}$$

- The target output P is the corresponding value of the composite unaliased image obtained using low-frequency acquisitions. The training error E is computed using the difference between the target and the computed output, as given by Eq. (8). When the training error $|E|$ reaches the pre-defined δ, in this case 10^{-3}, the weights $\mathbf{W}$ and $\tilde{\mathbf{W}}$ are frozen.

Reconstruction phase :

- The input feature vector $\mathbf{U_r}$ for the location (x,y) derived from the aliased coil images of acquisitions containing the entire range of k-space frequencies as

$$\mathbf{U_r} = \left[Re(S_1^{AH}(x,y)), Im(S_1^{AH}(x,y)), \ldots Re(S_8^{AH}(x,y)), Im(S_8^{AH}(x,y)), x, y\right] \quad (14)$$

- The output of the hidden layer, a vector of 98-dimensions ($\mathbf{V_r}$) comprises of elements computed as

$$v_{ri} \quad = \quad f\left(\sum_{j=1}^{18} w_{ij} u_{rj}\right) \quad i = 1, 2, \cdots, 98 \qquad (15)$$

- The output of the trained neural network $\hat{S}$ is computed as

$$\hat{S} = f\left(\sum_{j=1}^{98} \tilde{w}_j v_{rj}\right) \qquad (16)$$

- The outputs put together from each and every location, form the reconstructed image, which is an estimate of the true image S.

References

[1] K. P. Pruessmann, M. Weiger, M. B. Scheidegger, P. Boesiger, SENSE : Sensitivity encoding for fast MRI, Magnetic Resonance in Medicine 42 (5) (1999) 952–962.

[2] G. H. Glover, A. T. Lee, Motion artifacts in fMRI: comparison of 2DFT with PR and spiral scan methods, Magnetic Resonance in Medicine 33 (5) (2004) 624–635.

[3] K. P. Pruessmann, M. Weiger, P. Bornert, P. Boesiger, Advances in sensitivity encoding with arbitrary k-space trajectories, Magnetic Resonance in Medicine 46 (4) (2001) 638–651.

[4] T. Kidane, T. P. Eagan, Y. C. Cheng, T. N. Baig, V. Taracila, R. W. Brown, Matrix regularization for SENSE imaging, APS Meeting Abstracts (2003) C5001+.

[5] F. Lin, K. K. Kwong, J. W. Belliveau, L. L. Wald, Parallel imaging reconstruction using automatic regularization, Magnetic Resonance in Medicine 51 (3) (2004) 559–567.

[6] A. A. Samsonov, G. Eugene, Kholmovski, L. Dennis, Parker, C. R. Johnson, POCSENSE:POCS-based reconstruction for sensitivity encoded magnetic resonance imaging, Magnetic Resonance in Medicine 52 (6) (2004) 1397–1406.

[7] C. McKenzie, E. N. Yeh, M. A, Ohliger, M. D. Price, D. K. Sodickson, Self-Calibrating Parallel Imaging With Automatic Coil Sensitivity Extraction, Magnetic Resonance in Medicine 47 (3) (2002) 529–538.

[8] J. Petr, J. Kybic, M. Bock, S. Muller, V. Hlavac, Parallel image reconstruction using B-spline approximation (PROBER), Magnetic Resonance in Medicine 58 (3) (2007) 582–591.

[9] D. K. Sodickson, W. J. Manning, Simultaneous acquisition of spatial harmonics (SMASH): ultra-fast imaging with radio frequency coil arrays, Magnetic Resonance in Medicine 38 (4) (1997) 591–603.

[10] M. A. Griswold, P. M. Jakob, R. M. Hedemann, M. Nittka, V. Jellus, J. Wang, B. Keifer, A. Haase, Generalized autocalibrating partially parallel acquisitions (GRAPPA), Magnetic Resonance in Medicine 47 (6) (2002) 1202–1210.

[11] M. A. Griswold, R. M. Heidemann, P. M. Jakob, Direct parallel imaging reconstruction of radially sampled data using GRAPPA with relative shifts, Proceedings of 11th ISMRM (2003) 2349–2349.

[12] K. A. Heberlein, Y. Kadah, X. Hu, Segmented spiral parallel imaging using GRAPPA, Proceedings of 12th ISMRM (2004) 328–328.

[13] K. Heberlein, X. Hu, Auto-calibrated parallel imaging using dual-density spirals, Proceedings of 2nd International Workshop on Parallel MRI, Zurich (2004) 59–59.

[14] K. Heberlein, X. Hu, Auto-calibrated parallel spiral imaging, Magnetic Resonance in Medicine 55 (3) (2006) 619–625.

[15] E. N. Yeh, C. A. McKenzie, M. A. Ohliger, D. K. Sodickson, 3Parallel Magnetic Resonance Imaging with Adaptive Radius in k-Space (PARS):

Constrained Image Reconstruction using k-Space Locality in Radiofrequency Coil Encoded Data, Magnetic Resonance in Medicine 53 (6) (2005) 1383–1392.

[16] J. Sngas, T. Knopp, H. Eggers, dSENSE: Direct k-space reconstruction for non-Cartesian parallel MR imaging, Proceedings of 14th ISMRM (2006) 3652–3652.

[17] P. Hu, C. H. Meyer, BOSCO: Parallel image reconstruction based on successive convolution operations, Proceedings of 14th ISMRM (2006) 10–10.

[18] W. E. Kyriakos, L. P. Panych, D. F. Kacher, C. F. Westin, S. M. Bao, R. V. Mulkern, F. A. Jolesz, Sensitivity profiles from an array of coils for encoding and reconstruction in parallel (SPACERIP), Magnetic Resonance in Medicine 44 (2) (2000) 301–308.

[19] M. Buehrer, P. Boesiger, S. Kozerke, A fast approach to processing coil sensitivity maps using a neural network, Proceedings of 14th ISMRM (2006) 3657–3657.

[20] M. Reczko, D. Karras, B. Mertzios, D. Graveron-Demilly, D. van Ormondt, Improved MR image reconstruction from sparsely sampled scans based on neural networks, Pattern Recognition Letters 22 (2001) 35–46.

[21] J. J. Jackson, C. H. Meyer, D. G. Nishimura, A. Macovski, Selection of a convolution function for Fourier inversion using gridding, IEEE Transactions of Medical Imaging 10 (3) (1991) 473–478.

[22] Z. Wang, A. C. Bovik, H. R. Sheikh, E. P. Simoncelli, Image quality assessment: From error visibility to structural similarity, IEEE Transactions on Image Processing 13 (4) (2004) 600–612.

[23] K. A. Salem, D. L. Wilson, A human vision model for the objective evaluation of perceived image quality applied to MRI and image restoration, Proceedings of SPIE 4791 (2002) 412–415.

[24] J. X. Ji, J. B. Son, S. D. Rane, Pulsar: A matlab toolbox for parallel magnetic resonance imaging using array coils and multiple channel receivers, Concepts in Magnetic Resonance Part B: Magnetic Resonance Engineering 31 (1) (2007) 24–36.

[25] K. T. Block, J. Frahm, Spiral imaging: A critical appraisal, Journal of Magnetic Resonance Imaging 21 (2005) 657–668.

[26] D. E. Rumelhart, G. E. Hinton, R. J. Williams, Learning representations by back-propagating errors, Nature 323 (1986) 533–536.